This article has been accepted for publication in IEEE Internet of Things Journal. This is the author's version which has not been fully edited and content may change prior to final publication. Citation information: DOI 10.1109/JIOT.2024.3455577

Cascaded FSO systems with Optical Reflecting Surfaces

Narendra Vishwakarma, *Student Member, IEEE,* Swaminathan R., *Senior Member, IEEE,* Panagiotis D. Diamantoulakis, *Senior Member, IEEE,* and George K. Karagiannidis, *Fellow, IEEE*

***Abstract*—Recently, reconfigurable intelligent surfaces (RISs) have emerged as a highly promising technology within the realm of wireless communication systems, as they offer the potential to minimize obstructions, enhance reliability, and establish alternative paths for signal propagation. This paper presents the performance of a free space optics (FSO) system empowered by multiple optical reflecting surfaces (ORSs) over a Gamma-Gamma turbulence-induced fading channel with pointing errors by considering imperfections in channel state information (CSI). The expressions for probability density function (PDF) of the end-to-end FSO channel considering both perfect and imperfect CSI cases are derived. Further, the unified PDF and cumulative distribution function (CDF) of instantaneous signal-to-noise ratio (SNR) are determined under two detection schemes, i.e., intensity modulation/ direct detection and heterodyne detection for both perfect and imperfect CSI cases. Utilizing the derived CDFs, the closed-form expressions for outage probability and average symbol error rate (SER) of the proposed multiple ORSs system are obtained along with performing asymptotic analysis. Finally, the numerical results indicate that the performance of ORS-assisted FSO systems is significantly degraded by severe turbulence, pointing errors, and imperfect CSI. However, the inclusion of ORSs and increasing their number improves the performance of ORS-assisted FSO systems in the presence of turbulence, pointing errors, and imperfect CSI, compared to FSO systems without ORSs.**

***Index Terms*—Average SER, free space optics (FSO), imperfect channel state information (CSI), optical reflecting surface (ORS), pointing errors, selection scheme**

I. Introduction

The use of reconfigurable intelligent surface (RIS) has been regarded as one of the candidate enablers for sixth-generation (6G) wireless communications to provide extremely high reliability and improved remote area coverage with minimal power consumption [1]. RISs consist of passive planar surfaces, composed of reconfigurable elements, which will enable the manipulation of electromagnetic waves by adjusting the reflection properties [2]. By actively controlling the phase and amplitude of the reflected signals, RISs can optimize the signal propagation and mitigate the effects of blockages and interference in wireless communication networks [3], [4]. Depending upon their configurations, the reflecting surfaces can be reconfigurable or non-reconfigurable. The deployment of RISs offers a cost-effective solution to enhance wireless communication system performance by providing an alternate propagation path and improving reliability [5], [6]. Further, RISs can be deployed in various scenarios, including indoor and outdoor environments, to overcome obstacles and extend coverage area [7].

The radio frequency (RF) electromagnetic spectrum is currently experiencing a shortage, while it needs license and dedicated spectrum allocation which is costly. Moreover, the increasing demand for high-speed and reliable wireless communication has led to the exploration of alternative technologies that can overcome the limitations of traditional RF systems [8]. In this regard, free space optics (FSO) has emerged as a promising solution that offers several compelling advantages over RF-based systems, such as higher transmission data rates, huge bandwidth, and unlicensed spectrum [9]. Further, FSO also offers immunity to RF interference, as it operates in the optical domain. The FSO systems can be employed in applications such as point-to-point links, backhaul cellular networks, non-terrestrial networks, metropolitan area networks, campus connections, and last-mile connectivity [10]. Nevertheless, the FSO communication suffers from various atmospheric losses, including atmospheric turbulence-induced fading and pathloss, which limits the FSO performance. The atmospheric conditions, such as fog, rain, and snow, can introduce losses in FSO communication due to absorption, scattering, and beam spreading. Moreover, the FSO communication can be significantly affected by the pointing errors which are caused by the misalignment of the transmitting aperture and receiving apertures [11].

In literature, several techniques were proposed to overcome the limitations of the FSO systems, including spatial diversity techniques, multiple-input multiple-output (MIMO), relaying schemes, cooperative diversity, and hybrid FSO/RF system [12]–[19]. The diversity combining schemes such as maximal-ratio combining (MRC) and selection combining were proposed to alleviate the effect of atmospheric turbulence and adverse weather conditions in the FSO system [14], [15]. The authors in [16] examined the performance of a dual-

This research is supported by the National Research Foundation, Singapore under its Competitive Research Programme (NRF-CRP23-2019-0005), the National Research Foundation, Singapore and Infocomm Media Development Authority under its Future Communications Research & Development Programme (FCP-NTU-RG-2022-014), and MATRICS scheme (File No. MTR/2021/000553) of SERB, Govt. of India.

Narendra Vishwakarma is with the School of Computer Science and Engineering, Nanyang Technological University (NTU), Singapore 639798, (e-mail: narendra.vishwakarma@ntu.edu.sg)

Swaminathan R is with Department of Electrical Engineering, Indian Institute Technology Indore (IIT) Indore, (e-mail: swamiramabadran@iiti.ac.in)

Panagiotis D. Diamantoulakis and George K. Karagiannidis are with Department of Electrical and Computer Engineering, Aristotle University of Thessaloniki, Greece. George K. Karagiannidis is also with Artificial Intelligence & Cyber Systems Research Center, Lebanese American University (LAU), Lebanon. (e-mails: padiaman@auth.gr, geokarag@auth.gr)

This article has been accepted for publication in IEEE Internet of Things Journal. This is the author's version which has not been fully edited and
content may change prior to final publication. Citation information: DOI 10.1109/JIOT.2024.3455577

hop (DH) FSO system in which communication between a source and destination takes place with a relay positioned in between them. Moreover, in [17], the multiple relays were considered for the FSO system to enhance the coverage and improve the reliability of FSO link. In previous works [18], the relay-assisted mixed FSO/RF systems were investigated with the objective of improving performance and extending the coverage range of FSO communication systems. Further, in [19], the authors proposed a hybrid FSO/RF system, which complements the FSO link with a more reliable RF link to minimize the losses and improve the reliability of the FSO link. In [20], a comprehensive performance of a MIMO-based hybrid FSO/RF was presented, where both FSO and RF subsystems consist of multiple apertures/antenna on the transmitter and receiver side. Furthermore, in [21], the challenge of establishing end-to-end connectivity in internet-of-things (IoT) networks for data collection from remote areas is addressed. An IoT network is integrated with a wireless backhaul link, using a self-configuring protocol for aggregate node selection to transmit data to unmanned aerial vehicles (UAVs) over the hybrid transmission scheme, which employs millimeter-wave (mmWave), FSO, and terahertz (THz) technologies.

A. Related Literature

To mitigate the losses that occur due to atmospheric turbulence, poor weather conditions, and obstructions in the propagation channel, the RIS technology has been recently proposed for FSO communications [21]–[23], which is analogous to the RIS in RF wireless systems. The RISs comprise meta-surfaces, which can be classified into two distinct categories: reconfigurable and non-reconfigurable surfaces. This classification is contingent upon their respective configurations subsequent to the fabrication process. Furthermore, the optical RIS-aided FSO system possesses a notable advantage in terms of reduced hardware costs when compared to the relay-based systems [24]. This cost reduction is attributable to the absence of active components such as power amplifiers, encoders, decoders, etc., which are required in the relay-based system, however unnecessary in the context of the passive RIS-aided system. In [25] and [26], a dual transceiver FSO communication system and a RIS-assisted FSO system, respectively, are presented for smart city applications, specifically for high-speed trains. These systems enhance coverage, reduce handover frequency, and improve connectivity compared to direct and relay-assisted setups. Leveraging advanced channel models and performance evaluations, the RIS-assisted FSO systems demonstrated superior efficiency over relay-assisted models, significantly reducing base station requirements, capital expenditures, and the number of handover processes.

In [27], the authors have developed a statistical model for RIS-aided FSO system, which includes turbulence, geometric, and misalignment losses. Similarly, in [28], the statistical modeling of an RIS-aided multi-link FSO channel was developed by considering position, size and orientation of optical RIS with its phase shift profile. In [29], the authors studied the performance of a RIS-assisted FSO system to address the problem of skip zones and blockages in the line-of-sight (LOS) path of terrestrial FSO communication. Further, the performance of the RIS-assisted FSO system was investigated by considering the impact of turbulence and pointing errors. In [30], the authors proposed a RIS-assisted FSO system to mitigate the effects of atmospheric turbulence, pointing errors, and signal blockage. By evaluating the bit error rate (BER), outage probability, and channel capacity, the study demonstrated significant performance improvements in obstructed environments. This approach provides reliable connectivity for smart-city applications, especially in urban areas with dense populations and high-rise buildings. A comprehensive performance of an FSO system aided by RIS was demonstrated in [31] over different FSO channel turbulence models, where a single RIS with multiple elements was used to improve the FSO performance. In [32], the authors have extended the use of RIS in high-altitude platform (HAP)-aided backhaul network for FSO communication system. Moreover, in [32], the performance of the RIS-aided FSO system was evaluated in terms of performance metrics such as outage probability, outage capacity, and average bit error rate.

In [33], the authors have introduced a RIS-assisted multi-hop FSO system. The system architecture comprises a series of consecutive hops, wherein each hop is established as a RIS-assisted FSO link and it adopts decode-and-forward relaying technique to decode the received bits at the relay nodes. In [34], an optical reflecting surface (ORS)-aided MIMO-FSO communication system was proposed to mitigate the necessity for a LOS path in FSO communication. Further, the authors derived the bounds on the average BER and ergodic capacity by employing optical space shift keying (OSSK) technique. In [35], the authors have proposed a RIS-assisted mixed FSO/RF system, where there are multiple number of RIS-assisted RF source and the signal is transmitted from these RIS-aided RF sources to a relay node and the FSO link (without RIS) is used from relay to the destination node. Further, in [36], a RIS-assisted hybrid FSO/RF system was proposed in which both FSO and RF links are empowered by the single RIS and the performance of the hybrid FSO/RF system was investigated using the central limit theorem (CLT) approximation.

Due to channel estimation errors, it is often challenging to acquire a complete channel state information (CSI) in practice. Since the wireless channel varies rapidly due to fading and atmospheric attenuation, it is nearly impossible to acquire the perfect CSI at the source without any error [37], [38]. Therefore, it is crucial to study the impact of channel estimation errors on the performance of the system [39]. In [40], performance analysis of the FSO system was carried out by including the impact of imperfect CSI over the Fisher-Snedecor ($\mathcal{F}$) turbulence channel model. Further, the authors in [41] investigated the FSO system empowered by a single RIS by assuming imperfect CSI over the $\mathcal{F}$-distribution model. To improve the FSO system performance assisted by a single optical reflecting surface (ORS), where ORS is a special case of optical RIS when it operates as a perfect mirror [42], it is mandatory to consider multiple ORSs between source and destination in a backhaul network scenario. Recently, in [42], we have investigated the performance of multiple ORSs-assisted FSO system for a perfect CSI case.

This article has been accepted for publication in IEEE Internet of Things Journal. This is the author's version which has not been fully edited and
content may change prior to final publication. Citation information: DOI 10.1109/JIOT.2024.3455577

B. Motivations and Contributions

In previous works [29], [31], [35], [41], the analysis of RIS-assisted FSO system was carried out by assuming perfect and imperfect CSI cases over a single reflecting surface. Further, in [42], the performance of multiple ORSs-assisted FSO system was investigated for a perfect CSI case. However, the channel imperfections in the FSO link have been ignored and a detailed convergence test on the derived expressions is missing in [42]. Moreover, in practice, achieving perfect CSI for FSO channels is impractical due, mainly due to channel estimation errors. In this work, we have considered the multiple ORSs-assisted FSO system assuming both perfect and imperfect CSI cases. Here, the cascaded channel gain is modeled by taking turbulence, pointing errors, and imperfections in CSI into consideration. Since the imperfect channel gain includes the cascaded channel with CSI errors, are random in nature, deriving the closed-form expression for the probability density function (PDF) is challenging and is not straightforward. To the best of our knowledge, the unified PDF and CDF statistics for the instantaneous SNR of the multiple ORSs-assisted FSO system under imperfect CSI condition as well as the performance of multiple ORSs-assisted FSO system with imperfect CSI has not been analyzed in the existing literature. Note that the proposed work is the first work to consider the performance of multiple ORSs-assisted FSO system under imperfect CSI condition. Table I provides a summary of the current literature status on the performance of various RIS-based RF and FSO wireless systems.

The major contributions of this work are as follows:

- A multiple ORSs-aided FSO system is proposed, which comprises a multi-laser transmitter at the source and a single lens with photo-detector (PD) at the receiver, considering an ORS selection scheme to select the best possible ORS.
- Specifically, the exact expression for PDF of the cascaded FSO channel by including turbulence, pointing errors, and imperfect CSI is derived. Using the derived PDF expression, the unified PDF and cumulative distribution function (CDF) of overall instantaneous signal-to-noise ratio (SNR) for both perfect and imperfect CSI conditions are obtained.
- The closed-form expressions for the outage probability and average symbol error rate (ASER) of the proposed multiple ORSs-assisted system are determined based on the obtained statistical functions. In addition, an asymptotic analysis has been carried out in order to obtain the slope of the performance curves in the high-SNR region.
- Based on the numerical and simulation results, the performance of the proposed system is compared with single ORS-assisted and multi-relay-assisted FSO systems. Finally, Monte-Carlo simulations are performed to validate the derived outage and ASER expressions.

C. Organization of the Paper

The remainder of the paper is organized as follows: Section II introduces the system and channel models for the multiple ORSs-assisted FSO system and end-to-end channel PDF statistics are obtained under both perfect and imperfect CSI conditions. In Section III, the expressions for PDF and CDF of instantaneous SNR of the system are derived. In Section IV, the outage probability and average symbol error rate of the proposed system are examined for both perfect and imperfect CSI scenarios. Further, in Section IV, the asymptotic analysis is presented with convergence test for the derived expressions and the diversity gain of the multiple ORSs-assisted FSO system is determined. Furthermore, Section V offers numerical results along with important inferences and technical insights. Lastly, a conclusive summary of the paper is provided in Section VI.

II. System and Channel Models

A. System Model

We consider a multiple ORSs-assisted FSO system assuming N transmitting apertures, which are oriented to the respective ORSs and are capable of transmitting the FSO signal to N respective ORSs[1] as shown in Fig. 1. It is assumed that the ORS acts as a perfect mirror [2], which redirects the incident FSO signals to the receiving aperture [27], [34]. Here, we also assume that there is no direct LOS path exists between source (S) and destination (D). It is to be noted that before each transmission phase, the instantaneous SNR values of multiple ORSs-assisted FSO links are estimated at the receiver. From the available instantaneous SNR values, the index of the best ORS, which has the maximum instantaneous SNR, will be communicated to the transmitter using a perfect feedback link. After that the transmitter aperture corresponding to the best ORS will send the information signal to the receiver. Now the received signal of the j^{th} selected ORS link at D is expressed as

$$y_j = \mathcal{R} P_f I_j x_j + n_j, \tag{1}$$

where $j \in \{1, 2, \cdots, N\}$, y_j is the output signal, x_j denotes the input signal, P_f is the transmit power of the FSO signal, $\mathcal{R}$ represents the responsivity of the photo-detector, I_j is the cascaded FSO channel from transmitter to receiver via j^{th} ORS, and n_j is the additive white Gaussian noise (AWGN) with zero-mean and variance equal to σ_n^2.

B. Channel Model

The overall cascaded FSO channel from transmitter to receiver through j^{th} ORS is written as

$$I_j = I_{a_{1j}} I_{a_{2j}} I_{pj} I_{\ell j} I_{r_j}, \tag{2}$$

where $I_{a_{1j}}$ and $I_{a_{2j}}$ denote the atmospheric turbulence from transmitter aperture to j^{th} ORS and j^{th} ORS to receiver aperture, respectively, I_{pj} is the pointing error coefficient for j^{th} ORS-aided link, and $I_{\ell j}$ denotes the path-loss factor.

[1]The placement of the ORS on the building in the figure is shown for illustrative proposes. However, the ORSs can also be positioned on different buildings based on the source and destination locations.

[2]In this scenario, the ORS is positioned in such a way that the angle of incidence is equal to the angle of reflection so that the phase shift introduced by the ORS is precisely countered using the phase-shift profile. Hence, in this configuration, the ORS functions like a reflective mirror [27], [34].

TABLE I: Summary of literature on models for RIS-aided systems

Ref.	System model	Number of RIS	Modulation technique	FSO/RF channel	CSI	Performance Metrics
[2]	RIS-aided RF system	Single	M-ary PSK	Rayleigh	Perfect CSI	ASEP
[5]	Cascaded RIS-assisted RF system	Multiple	Binary modulation schemes	Nakagami-m	Perfect CSI	OP, EC, ASEP
[26]	RIS-FSO	Multiple	NA	Lognormal, Gamma-Gamma	Perfect CSI	Average SNR and OP
[30]	RIS-FSO	Single	Binary PSK	Gamma-Gamma	Perfect CSI	OP, EC, ASER
[39]	Multiple RIS-assisted RF system	Multiple	Binary modulation schemes	Nakagami-m	Imperfect CSI	EC, ASEP
[29]	RIS-aided FSO system	Single	Binary modulation schemes	Gamma–Gamma	Perfect CSI	OP, ABER, EC
[31]	RIS-assisted FSO system	Single	Binary modulation schemes	Gamma–Gamma, $\mathcal{F}$-distribution, Malaga	Perfect CSI	OP, ABER, EC
[32]	HAPS-based RIS-assisted FSO system	Single	M-ary PSK	$\mathcal{F}$-distribution	Perfect CSI	ASER, channel capacity
[35]	RIS-aided mixed FSO/RF with relay network	Two	Binary PSK	Gamma–Gamma/ Rayleigh	Perfect CSI	OP, ASEP
[36]	RIS-assisted hybrid FSO/RF system	Two	Binary PSK	Gamma–Gamma/ Rayleigh	Perfect CSI	OP, ABER, EC
[41]	RIS-aided FSO system	Single	Binary modulation schemes	$\mathcal{F}$-distribution	Imerfect CSI	OP, ABER, EC

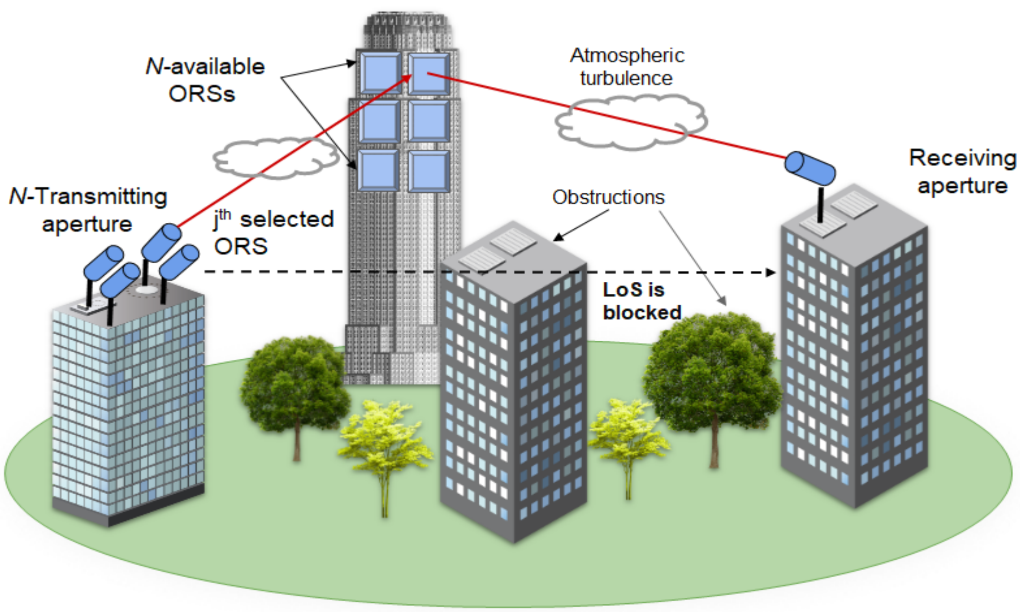

Fig. 1: Selection-based multiple ORSs-assisted FSO system model

Further, $I_{\ell j}$ is a constant, which follows the Beers Lambert law and is expressed as $I_{\ell j} = \exp(-\Omega_\ell L_j)$, where Ω_ℓ is the attenuation coefficient and L_j is the end-to-end distance for any j^{th} ORS-aided FSO link. In (2), $I_{r_j} = \chi_j e^{i(\Delta\psi_o^{(j)}(z)-\pi)}$ represents attenuation due to ORS, where χ_j is the amplitude reflection coefficient and $\Delta\psi_o^{(j)}$ is the phase induced by the j^{th} ORS. The phase can be calculated using the phase-shift profile as $\Delta\psi_o^{(j)}(z) = \pi + z_j k_0(\sin\theta_d - \sin\theta_r)$ [27, eq. (13)]. Here, k_0 is the wave number and z_j is the position of the ORS, Further, θ_d and θ_r represent the angle of incident and angle of reflection, respectively. For the ORS to act as a perfect mirror, $\chi_j = 1$ and $\theta_d = \theta_r$. This results in a constant phase shift of π, simplifying I_{r_j} to 1.

It is to be noted that the channel turbulence coefficient $I_{a_{1j}}$ is modeled in a similar manner to $I_{a_{2j}}$. However, we consider a general scenario where the turbulence coefficients $I_{a_{1j}}$ and $I_{a_{2j}}$ are independently but non-identically distributed (i.n.i.d). Furthermore, $L_j = L_{1j} + L_{2j}$, where L_{1j} and L_{2j} are distances from S to j^{th} ORS and j^{th} ORS to D, respectively.

1) Atmospheric Turbulence Model: The turbulence of the FSO channel is modeled using Gamma-Gamma distribution and its PDF is given by [29]

$$f_{I_{a_{ij}}}(x) = \frac{x^{-1}}{\Gamma(\alpha_{ij})\Gamma(\beta_{ij})} G_{0\,2}^{2\,0}\left(\alpha_{ij}\beta_{ij}x \middle| \begin{matrix} - \\ \alpha_{ij}, \beta_{ij} \end{matrix}\right), \quad (3)$$

This article has been accepted for publication in IEEE Internet of Things Journal. This is the author's version which has not been fully edited and content may change prior to final publication. Citation information: DOI 10.1109/JIOT.2024.3455577

TABLE II: List of notations used in the paper

$C_j = \frac{\alpha_{1j}\beta_{1j}\alpha_{2j}\beta_{2j}}{I_{\ell j}A_j}$	$B_j = \frac{\rho_j}{\Gamma(\alpha_{1j})\Gamma(\beta_{1j})\Gamma(\alpha_{2j})\Gamma(\beta_{2j})}$	$P_1 = n + \alpha_{1j} + \alpha_{2j} + \beta_{1j} + \beta_{2j} - 5$
$\mathcal{X}_{1j} = [\alpha_{2j}, \beta_{2j}, \alpha_{1j}, \beta_{1j}]$	$\mathcal{X}_{2j} = [\rho_j, \alpha_{2j}, \beta_{2j}, \alpha_{1j}, \beta_{1j}]$	$G_{1j} = G\,_{10}^{1}\,_{3}^{10}\left(\frac{2^8 K_2 \delta^2}{C_j}\middle\vert \begin{matrix}\mathcal{X}_{3j}\\ \mathcal{X}_{4j}\end{matrix}\right)$
$\mathcal{X}_{3j} = \left[\frac{1-\rho_j}{2}, \frac{2-\rho_j}{2}, \frac{1-\alpha_{2j}}{2}, \frac{2-\alpha_{2j}}{2}, \frac{1-\beta_{2j}}{2}, \frac{2-\beta_{2j}}{2}, \frac{1-\alpha_{1j}}{2}, \frac{2-\alpha_{1j}}{2}, \frac{1-\beta_{1j}}{2}, \frac{2-\beta_{1j}}{2}\right]$		$\mathcal{X}_{4j} = \left[\frac{n}{2}, \frac{-\rho_j}{2}, \frac{1-\alpha_{2j}}{2}\right]$
$\mathcal{X}_{5k} = [(\rho_k + 1, 1)]$	$\mathcal{X}_{6k} = [(\rho_k, 1), (\alpha_{2k}, 1), (\beta_{2k}, 1), (\alpha_{1k}, 1), (\beta_{1k}, 1)]$	$\mathcal{X}_{7i} = [(1, 1), (\rho_i + 1, 1)]$
$\mathcal{X}_{8i} = [(\rho_i, 1), (\alpha_{2i}, 1), (\beta_{2i}, 1), (\alpha_{1i}, 1), (\beta_{1i}, 1), (0, 1)]$		$P_2 = \alpha_{1j} + \alpha_{2j} + \beta_{1j} + \beta_{2j} - 5$

where $i \in \{1, 2\}$, α_{ij} and β_{ij} denote the large-scale and small-scale turbulence parameters [29], respectively, and $G\,_{p}^{m}\,_{q}^{n}(\cdot)$ represents the Meijer G-function [43, 9.301].

2) Pointing Errors Model: The pointing errors in the FSO system aided with ORS are attributed to beam jitter and ORS jitter. The expression for PDF of end-to-end pointing errors for an ORS-assisted FSO channel can be written as [22, eq. (12)]

$$f_{I_{pj}}(x) = \frac{\rho_j}{A_j^{\rho_j}} x^{\rho_j - 1}, \quad 0 \le x \le A_j, \tag{4}$$

where $A_j = [\text{erf}(\upsilon_j)]^2$, $\upsilon_j = \frac{\sqrt{\pi}a_0}{\sqrt{2}W_{z_j}}$, $W^2_{z^{(j)}_{eq}} = \frac{W^2_{z_j}\sqrt{\pi}\text{erf}(\upsilon_j)}{2\upsilon_j\exp(-\upsilon_j^2)}$. Here, a_0 is the aperture radius and W_{z_j} denotes the beam width, which is given by $W_{z_j} = \phi_{d_j}L_j$, where ϕ_{d_j} denotes the beam divergence angle. Further in (4), $\rho_j = \frac{W^2_{z^{(j)}_{eq}}}{4L_j^2\sigma^2_{\theta_j} + 16L^2_{2j}\sigma^2_{\varphi_j}}$ is the pointing error coefficient, where $\sigma^2_{\theta_j}$ and $\sigma^2_{\varphi_j}$ are the variances corresponding to displacement angles at the transmitter and the ORS, respectively [22].

3) PDF of End-to-End FSO Channel: The PDF of overall FSO channel, including end-to-end turbulence and pointing errors, can be expressed as

$$f_{I_j}(t) = \int_{\frac{t}{I_{\ell j}A_j}}^{\infty} \frac{1}{I_{\ell j}y} \int_0^{\infty} \frac{1}{x} f_{I_{a_{1j}}}(x) f_{I_{a_{2j}}}\left(\frac{y}{x}\right) f_{I_{pj}}\left(\frac{t}{I_{\ell j}y}\right) dx dy. \tag{5}$$

The inner integral is evaluated by substituting (3) in (5) and using [44, eq. (07.34.21.0013.01)], we get

$$f_{I_j}(t) = \int_{\frac{t}{I_{\ell j}A_j}}^{\infty} \frac{1}{I_{\ell j}y} \frac{y^{-1}}{\Gamma(\alpha_{1j})\Gamma(\beta_{1j})\Gamma(\alpha_{2j})\Gamma(\beta_{2j})} \times G\,_{0}^{4}\,_{4}^{0}\left(\alpha_{1j}\beta_{1j}\alpha_{2j}\beta_{2j}y \middle\vert \begin{matrix} - \\ \mathcal{X}_{1j}\end{matrix}\right) dy, \tag{6}$$

Further, we use [44, eq. (07.34.21.0085.01)] to get the final expression of channel gain as

$$f_{I_j}(t) = B_j t^{-1} G\,_{1}^{5}\,_{5}^{0}\left(C_j t \middle\vert \begin{matrix}\rho_j + 1\\ \mathcal{X}_{2j}\end{matrix}\right), \tag{7}$$

where C_j, B_j, and $\mathcal{X}_{2j}$ are given in Table II.

4) PDF of Imperfect Channel: In practical scenarios, the FSO channel is changing rapidly due to pointing errors and weather conditions like fog, smog, and rain. Due to this there will be channel estimations errors leading to imperfect CSI. Hence, the imperfect channel gain of the FSO link can be written as [40, eq. (10)]

$$\tilde{I}_j = \delta I_j + \sqrt{1 - \delta^2}\epsilon, \tag{8}$$

where $\delta \in [0, 1]$ represents the CSI correlation coefficient that determines the accuracy of channel estimation. A value of $\delta = 1$ indicates perfect CSI. Moreover, ϵ is a random variable denoting the errors due to imperfect CSI, which is independent of I_j, and follows a zero-mean Gaussian distribution with variance σ_e^2.

Theorem 1: The PDF of ORS-assisted FSO channel with imperfect CSI over Gamma-Gamma turbulence distribution and pointing errors is given by

$$f_{\tilde{I}_j}(t) = \begin{cases} \frac{B_j K_1}{\pi^2}\exp\left(-K_2 t^2\right) \sum_{n=0}^{\infty} \frac{2^{P_1} K_2^{\frac{n}{2}}}{n!} G_{1j} t^n, & t > 0 \\ 1 - I_0^{(j)}, & t = 0. \end{cases} \tag{9}$$

where

$$I_0^{(j)} = \frac{B_j K_1}{2\pi^2} \sum_{n=0}^{\infty} \frac{2^{P_1} K_2^{-\frac{1}{2}}}{n!} G_{1j} \Gamma\left(\frac{n+1}{2}\right). \tag{10}$$

Note that P_1 and G_{1j} are listed in Table II.

Proof: Please see Appendix A. ■

It is worth highlighting that, in contrast to the above channel PDF, previous work [41] on the RIS-assisted FSO system computes the imperfect channel statistics by assuming a single RIS without incorporating any combining scheme. Furthermore, in [42], the analysis involves multiple ORSs, but it neglects imperfect CSI, convergence test, and lacks the unification of both HD and IM/DD techniques.

III. SNR STATISTICS

The unified instantaneous SNR of the end-to-end j^{th} ORS-assisted FSO link with perfect CSI is given by $\gamma_j^{(r)} = |I_j|^r\gamma_0$, where $\gamma_0 = P_t/\sigma_n^2$ denotes average SNR, $r = 1$ and 2 represent HD and IM/DD techniques, respectively. Using the power transformations of random variable in (7), the PDF of γ_j is written as

$$f_{\gamma_j^{(r)}}(x) = \frac{B_j}{r} x^{-1} G\,_{1}^{5}\,_{5}^{0}\left(C_j\left(\frac{x}{\gamma_0}\right)^{\frac{1}{r}} \middle\vert \begin{matrix}\rho_j + 1\\ \mathcal{X}_{2j}\end{matrix}\right), \tag{11}$$

Further, the CDF of the γ_j is determined by using [44, 07.34.21.0084.01] and is given by

$$F_{\gamma_j^{(r)}}(x) = B_j G_{2\,6}^{5\,1}\left(C_j\left(\frac{x}{\gamma_0}\right)^{\frac{1}{r}}\middle|\begin{matrix}1,\rho_j+1\\ \mathcal{X}_{2j},0\end{matrix}\right), \quad (12)$$

Similarly, the instantaneous SNR of the FSO link having imperfect CSI is given by $\tilde{\gamma}_j^{(r)} = |\tilde{I}_j|^r\gamma_0$. Using the power transformations in (9), the PDF of γ_j is expressed as

$$f_{\tilde{\gamma}_j^{(r)}}(x) = \begin{cases}\frac{B_jK_1}{r\pi^2}e^{-\frac{K_2x^{2/r}}{\gamma_0^{2/r}}}\sum_{n=0}^{\infty}\frac{2^{P_1}K_2^{\frac{n}{2}}}{n!}G_{1j}\frac{x^{\left(\frac{n-r+1}{r}\right)}}{\gamma_0^{\frac{n+1}{r}}}, & x>0\\ 1-I_0^{(j)}, & x=0.\end{cases} \quad (13)$$

Now the CDF of $\tilde{\gamma}_j^{(r)}$ can be evaluated as $F_{\tilde{\gamma}_j^{(r)}}(x) = \int_0^x f_{\tilde{\gamma}_j^{(r)}}(t)dt$. By employing [44, 07.34.03.0228.01] and [44, 07.34.21.0084.01], the final expression for the CDF is given by

$$F_{\tilde{\gamma}_j^{(r)}}(x) = \frac{B_jK_1}{r\pi^2}\sum_{n=0}^{\infty}\frac{2^{P_1}K_2^{-\frac{1}{2}}}{n!}G_{1j}G_{1\,2}^{1\,1}\left(\frac{K_2x^{\frac{2}{r}}}{\gamma_0^{\frac{2}{r}}}\middle|\begin{matrix}1\\ \frac{n+1}{2},0\end{matrix}\right) + 1 - I_0^{(j)}. \quad (14)$$

IV. Performance Analysis

The outage probability and ASER for the proposed selection-based ORS-assisted FSO system with perfect CSI and imperfect CSI are discussed in this section.

A. With Perfect CSI

1) Outage Probability: For the proposed system, if the instantaneous SNR of the best ORS-assisted FSO link (i.e. link with maximum instantaneous SNR $\gamma_{\max}$) goes below a threshold SNR γ_T, then outage will occur. Now the outage probability of the proposed system is given by

$$P_o = \Pr(\gamma_{\max} < \gamma_T) = F_{\gamma_{max}}(\gamma_T), \quad (15)$$

where $\Pr(\cdot)$ denotes the probability operator and $F_{\gamma_{max}}(\cdot)$ is the CDF of γ_{max}.

Theorem 2: The CDF of the best ORS-assisted FSO link, which is having the maximum instantaneous SNR $\gamma_{\max}$ among the N available links, is given by

$$F_{\gamma_{max}}(\gamma) = \prod_{j=1}^{N} B_j G_{2\,6}^{5\,1}\left(C_j\left(\frac{\gamma}{\gamma_0}\right)^{\frac{1}{r}}\middle|\begin{matrix}1,\rho_j+1\\ \mathcal{X}_{2j},0\end{matrix}\right). \quad (16)$$

Proof: Please see Appendix B ■

By substituting $\gamma = \gamma_T$ in (16), the final expression for outage probability for perfect CSI case is given by

$$P_o^{(P)} = \prod_{j=1}^{N} B_j G_{2\,6}^{5\,1}\left(C_j\left(\frac{\gamma_T}{\gamma_0}\right)^{\frac{1}{r}}\middle|\begin{matrix}1,\rho_j+1\\ \mathcal{X}_{2j},0\end{matrix}\right). \quad (17)$$

The asymptotic expression for the outage probability is calculated by assuming $\gamma_0 \to \infty$ in (17). Further, by substituting the asymptotic expansion of the Meijer G-function using [44, eq. (07.34.06.0040.01)] and after simplifying, the asymptotic outage probability can be expressed as

$$P_o^{(P)^\infty} = \prod_{j=1}^{N} B_j \sum_{l=1}^{5}\frac{\prod_{\substack{m=1\\ m\neq l}}^{5}\Gamma(\mathcal{X}_{2j,m}-\mathcal{X}_{2j,l})}{\mathcal{X}_{2j,l}\Gamma(\rho_j+1-\mathcal{X}_{2j,l})} \times C_j^{\mathcal{X}_{2j,l}}\left(\frac{\gamma_T}{\gamma_0}\right)^{\mathcal{X}_{2j,l}/r}, \quad (18)$$

where $\mathcal{X}_{2j,l}$ is the l^{th} term of $\mathcal{X}_{2j}$.

2) Average Symbol Error Rate: The ASER of the proposed multiple ORSs-aided system is calculated as

$$\overline{P}_e^{(P)} = \int_0^\infty p(e/x)f_{\gamma_{\max}}(x)dx, \quad (19)$$

where $p(e/x)$ denotes the error probability for $\mathcal{M}$-ary phase-shift keying (MPSK) or $\mathcal{M}$-quadrature amplitude modulation (MQAM) schemes conditioned on the instantaneous SNR of the system [45]. Furthermore, the expression for $p(e/x)$ in terms of Fox's H-function is represented by [44, 07.34.26.0008.01]

$$p(e/x) = \frac{\mathcal{A}}{2\sqrt{\pi}}H_{1\,2}^{2\,0}\left(Q^2\gamma\middle|\begin{matrix}(1,1)\\ (0,1),(0.5,1)\end{matrix}\right), \quad (20)$$

In case of MPSK scheme, $\mathcal{A}=1$ for $\mathcal{M}=2$, $\mathcal{A}=2$ for $\mathcal{M}>2$, and $Q=\sin(\pi/\mathcal{M})$. For MQAM scheme, $\mathcal{A} = 4\frac{(\sqrt{M}-1)}{\sqrt{M}}$ and $Q=\sqrt{\frac{3}{2(\mathcal{M}-1)}}$ [45]. Here, $\mathcal{M}$ denotes the modulation order of the MPSK/MQAM schemes. Further, the PDF $f_{\gamma_{\max}}(\cdot)$ in (19) can be obtained by differentiating the CDF expression in (16) as

$$f_{\gamma_{\max}}(x) = \sum_{k=1}^{N}\prod_{j=1, j\neq k}^{N} f_{\gamma_k^{(r)}}(x)F_{\gamma_j^{(r)}}(x), \quad (21)$$

where $f_{\gamma_k^{(r)}}(\cdot)$ and $F_{\gamma_j^{(r)}}(\cdot)$ are expressed in (11) and (12), respectively. Moreover, the expression for (11) and (12) can be rewritten in the form of Fox's H-function using [44, 07.34.26.0008.01] and after replacing these expression in (19), the ASER is given by

$$\overline{P}_e^{(P)} = \frac{\mathcal{A}}{4\sqrt{\pi}}\prod_{j=1}^{N}B_j\sum_{k=1}^{N}\int_0^\infty \gamma^{-1}H_{1\,2}^{2\,0}\left(Q^2\gamma\middle|\begin{matrix}(1,1)\\ (0,1),(0.5,1)\end{matrix}\right) \times H_{1\,5}^{5\,0}\left(C_k\left(\frac{\gamma}{\gamma_0}\right)^{\frac{1}{r}}\middle|\begin{matrix}\mathcal{X}_{5k}\\ \mathcal{X}_{6k}\end{matrix}\right)\prod_{\substack{i=1\\ i\neq k}}^{N}H_{2\,6}^{5\,1}\left(C_i\left(\frac{\gamma}{\gamma_0}\right)^{\frac{1}{r}}\middle|\begin{matrix}\mathcal{X}_{7i}\\ \mathcal{X}_{8i}\end{matrix}\right)d\gamma. \quad (22)$$

In order to solve the above integral, first we expand the Fox's H-function using [46, eq. (1.2)] and then apply the Mellin's transformation theorem [47, eq. (1.29)]. Now, by utilizing the definition of multivariate Fox's H-function [46, eq. (A.1)], the ASER expression for proposed ORSs-aided system is given by (23).

This article has been accepted for publication in IEEE Internet of Things Journal. This is the author's version which has not been fully edited and content may change prior to final publication. Citation information: DOI 10.1109/JIOT.2024.3455577

$$\overline{P}_e^{(P)} = \frac{\mathcal{A}}{2r\sqrt{\pi}} \prod_{j=1}^{N} B_j \Bigg\{ H^{0,2:\ 5,0:\ 5,1:\cdots:\ 5,1}_{2,1:\ 1,5:\ 2,6:\cdots:\ 2,6} \left(\frac{C_1}{(Q^2\gamma_0)^{\frac{1}{r}}}, \cdots, \frac{C_N}{(Q^2\gamma_0)^{\frac{1}{r}}} \,\middle|\, \begin{matrix} \left(1;\{\frac{1}{r}\}_1^N\right), \left(0.5;\{\frac{1}{r}\}_1^N\right); \mathcal{X}_{31}; \mathcal{X}_{52}; \cdots; \mathcal{X}_{5N} \\ \left(0;\{\frac{1}{r}\}_1^N\right); \mathcal{X}_{41}; \mathcal{X}_{62}; \cdots; \mathcal{X}_{6N} \end{matrix} \right)$$
$$+ H^{0,2:\ 5,1:\ 5,0:\cdots:\ 5,1}_{2,1:\ 2,6:\ 1,5:\cdots:\ 2,6} \left(\frac{D_1}{(Q^2\gamma_0)^{\frac{1}{r}}}, \cdots, \frac{D_N}{(Q^2\gamma_0)^{\frac{1}{r}}} \,\middle|\, \begin{matrix} \left(1;\{\frac{1}{r}\}_1^N\right), \left(0.5;\{\frac{1}{r}\}_1^N\right); \mathcal{X}_{51}; \mathcal{X}_{32}; \cdots; \mathcal{X}_{5N} \\ \left(0;\{\frac{1}{r}\}_1^N\right); \mathcal{X}_{61}; \mathcal{X}_{42}; \cdots; \mathcal{X}_{6N} \end{matrix} \right) + \cdots$$
$$\cdots + H^{0,2:\ 5,1:\ 5,1:\cdots,:\ 5,0}_{2,1:\ 2,6:\ 2,6:\cdots:\ 1,5} \left(\frac{D_1}{(Q^2\gamma_0)^{\frac{1}{r}}}, \cdots, \frac{D_N}{(Q^2\gamma_0)^{\frac{1}{r}}} \,\middle|\, \begin{matrix} \left(1;\{\frac{1}{r}\}_1^N\right), \left(0.5;\{\frac{1}{r}\}_1^N\right); \mathcal{X}_{51}; \mathcal{X}_{52}; \cdots; \mathcal{X}_{3N} \\ \left(0;\{\frac{1}{r}\}_1^N\right); \mathcal{X}_{61}; \mathcal{X}_{62}; \cdots; \mathcal{X}_{4N} \end{matrix} \right) \Bigg\}. \quad (23)$$

Proposition 1: The asymptotic expression of the ASER for perfect CSI is given by

$$\overline{P}_e^{(P)^\infty} = \frac{\mathcal{A}}{2\sqrt{\pi}} \left(\frac{1}{Q^2\gamma_0}\right)^{\frac{1}{r}\sum_{s=1}^{N} P_s} \left[\frac{\Gamma\left(\frac{1}{2} + \frac{1}{r}\sum_{s=1}^{N} P_s\right)}{\sum_{s=1}^{N} P_s} \right.$$
$$\left. \times \sum_{k=1}^{N} \frac{1}{\prod_{\substack{i=1\\ i\neq k}}^{N} P_i} \prod_{j=1}^{N} \frac{\prod_{\substack{m=1\\ \mathcal{X}_{2j,m}\neq P_k}}^{5} \Gamma(\mathcal{X}_{2j,m} - P_j)}{\Gamma(\rho_j + 1 - P_j)} B_j C_j^{P_j} \right]. \quad (24)$$

Proof: The asymptotic expression for ASER is calculated by assuming $\gamma_0 \to \infty$ in (23) and the dominant poles are determined as $P_j = \min\{\rho_j, \alpha_{2j}, \beta_{2j}, \alpha_{1j}, \beta_{1j}\}$, where $j = 1, 2, \cdots, N$. Furthermore, there are a total of N poles associated with each term of multivariate Fox's H-function in (23). Finally, by calculating the residue at each dominate pole [42], the asymptotic expression for the ASER is obtained as (24) ∎

B. With Imperfect CSI

1) Outage Probability: Similar to outage of perfect CSI, the outage probability for the imperfect CSI case, by using (15), can be written as

$$P_o^{(I)} = \prod_{j=1}^{N} \Pr(\tilde{\gamma}_1^{(r)} < \gamma_T) \Pr(\tilde{\gamma}_2^{(r)} < \gamma_T) \cdots \Pr(\tilde{\gamma}_N^{(r)} < \gamma_T). \quad (25)$$

After simplification, we get

$$P_o^{(I)} = \prod_{j=1}^{N} F_{\tilde{\gamma}_j^{(r)}}(\gamma_T). \quad (26)$$

By replacing x with γ_T in (14) and substituting in (26), the final expression for outage probability in closed-form is given by

$$P_o^{(I)} = \prod_{j=1}^{N} \left[\frac{B_j K_1}{r\pi^2} \sum_{n=0}^{\infty} \frac{2^{P_1} K_2^{-\frac{1}{2}}}{n!} G_{1j} G^{1\,1}_{1\,2} \left(\frac{K_2 \gamma_T^{\frac{2}{r}}}{\gamma_0^{\frac{2}{r}}} \,\middle|\, \begin{matrix} 1 \\ \frac{n+1}{2}, 0 \end{matrix} \right) \right.$$
$$\left. + 1 - I_0^{(j)} \right]. \quad (27)$$

In order to calculate the asymptotic outage probability, we assume $\gamma_0 \to \infty$ in (27) and by using [44, eq. (07.34.06.0040.01)], we obtain the asymptotic outage probability as

$$P_o^{(I)^\infty} = \prod_{j=1}^{N} \left[\frac{B_j K_1}{\pi^2} \sum_{n=0}^{\infty} \frac{2^{P_1} K_2^n}{(n+1)!} G_{1j} \left(\frac{\gamma_T^{\frac{n+1}{r}}}{\gamma_0^{\frac{n+1}{r}}} \right) + 1 - I_0^{(j)} \right]. \quad (28)$$

Remark 1: By assuming $n = 0$ in (28), which is the dominant term in summation, a more simplified expression for $P_o^{(I)^\infty}$ is obtained and is given by

$$P_o^{(I)^\infty} = \prod_{j=1}^{N} \Bigg[\underbrace{\frac{B_j K_1}{\pi^2} 2^{P_1} G_{1j} \left(\frac{\gamma_T^{\frac{1}{r}}}{\gamma_0^{\frac{1}{r}}} \right)}_{T_1^P} + \underbrace{\left(1 - I_0^{(j)}\right)}_{T_2^P} \Bigg]. \quad (29)$$

It is important to note that (29) contains two terms, where the first term T_1^P depends on γ_0 and the second term T_2^P is a constant independent of γ_0. As a result, $T_2^P \gg T_1^P$ in the high-SNR region and the outage probability will attain a floor value, which is equal to

$$P_0^{\text{fixed}} = \prod_{j=1}^{N} \left(1 - I_0^{(j)}\right). \quad (30)$$

2) Average Symbol Error Rate: The ASER of the proposed system for sub-carrier IM-based MPSK signaling is obtained by utilizing the derived CDF $F_{\gamma_{max}^{(r)}}(x)$ and is given by [3]

$$\overline{P}_e^{(I)} = \frac{\mathcal{A}\sqrt{\mathcal{D}}}{2\sqrt{2\pi}} \int_0^{\infty} x^{-1/2} F_{\gamma_{max}^{(r)}}(x) e^{-\frac{\mathcal{D}x}{2}} dx, \quad (31)$$

where $\mathcal{A} = 1$, $\mathcal{D} = 2$ for $\mathcal{M}$=2 and $\mathcal{A} = 2$, $\mathcal{D} = 2\sin^2\left(\frac{\pi}{\mathcal{M}}\right)$ for $\mathcal{M}$ >2. Since the evaluation of the above integral is complicated, we have used a Gauss-Laguerre quadrature approximation [48] and the final ASER expression can be evaluated as

$$\overline{P}_e^{(I)} = \frac{\mathcal{A}\sqrt{\mathcal{D}}}{2\sqrt{2\pi}} \sum_{k=1}^{m} W_k \prod_{j=1}^{N} F_{\gamma_j^{(r)}}(\varphi_k), \quad (32)$$

where W_k denotes the weight coefficient and is expressed as

$$W_k = \frac{\varphi_k \Gamma(m + 0.5)}{m!(m+1)^2 (L_{m+1}^{-1/2}(\varphi_k))^2}. \quad (33)$$

In (32), φ_k is the k^{th} zero of the Laguerre polynomial $L_m^{-1/2}(\cdot)$, which is given as [43, eq. (8.970.1)]

$$L_m^{-1/2}(y) = \sum_{l=0}^{m} \binom{m - \frac{1}{2}}{m - l} \frac{(-y)^l}{l!}. \quad (34)$$

Proposition 2: The asymptotic expression of ASER for imperfect CSI case is given by

$$\overline{P}_e^{(I)^\infty} = \frac{\mathcal{A}\sqrt{\mathcal{D}}}{2\sqrt{2\pi}} \sum_{k=1}^{m} W_k \prod_{j=1}^{N} \left\{ \frac{B_j K_1}{\pi^2} \sum_{n=0}^{\infty} \frac{2^{P_1} K_2^n}{(n+1)!} G_{1j} \frac{\varphi_k^{\frac{n+1}{r}}}{\gamma_0^{\frac{n+1}{r}}} + \left(1 - I_0^{(j)}\right) \right\}. \tag{35}$$

Proof: By assuming $\gamma_0 \to \infty$ in (32) and employing [44, eq. (07.34.06.0040.01)] similar to outage, the asymptotic ASER expression is written as

$$\overline{P}_e^{(I)^\infty} = \frac{\mathcal{A}\sqrt{\mathcal{D}}}{2\sqrt{2\pi}} \sum_{k=1}^{m} W_k \prod_{j=1}^{N} F^{\infty}_{\gamma_j^{(r)}}(\varphi_k), \tag{36}$$

By substituting $\gamma_T = \varphi_k$ in the asymptotic outage expression for imperfect CSI, given by (29), the asymptotic CDF $F^{\infty}_{\gamma_j^{(r)}}(\varphi_k)$ can be obtained. Therefore, the final expression for asymptotic ASER is obtained as (35). ■

Remark 2: Using the dominant term in (35) by substituting $n = 0$, a more simpler asymptotic ASER expression is obtained, which is given by

$$\overline{P}_e^{(I)^\infty} = \frac{\mathcal{A}\sqrt{\mathcal{D}}}{2\sqrt{2\pi}} \sum_{k=1}^{m} W_k \times \prod_{j=1}^{N} \left\{ \underbrace{\frac{B_j K_1}{\pi^2} 2^{P_2} G_{1j} \frac{\varphi_k^{\frac{1}{r}}}{\gamma_0^{\frac{1}{r}}}}_{T_1^s} + \underbrace{\left(1 - I_0^{(j)}\right)}_{T_2^s} \right\}. \tag{37}$$

Similar to outage probability, the first term T_1^s in (37) depends on γ_0 and the second term T_2^s is a constant. Since $T_2^s \gg T_1^s$ in the high-SNR region, ASER will also approach to a floor value equal to

$$P_{ser}^{\text{fixed}} = \frac{\mathcal{A}\sqrt{\mathcal{D}}}{2\sqrt{2\pi}} \sum_{k=1}^{m} W_k \prod_{j=1}^{N} \left(1 - I_0^{(j)}\right). \tag{38}$$

C. Convergence Test

In order to examine the convergence of the obtained outage and ASER expressions for imperfect CSI case, as presented in (27) and (32), respectively, a Cauchy ratio test is conducted on the power series of the CDF of $\tilde{\gamma}_j^{(r)}$, as given in (14). This CDF expression is used for calculating the outage probability and ASER expressions. Subsequently, if the infinite series in $F_{\tilde{\gamma}_j^{(r)}}(x)$ exhibits convergence, then both outage (i.e. eq. (27)) and ASER (i.e. eq. (32)) will be absolutely convergent. In order to demonstrate absolute convergence, an infinite series, such as $\sum_{m=0}^{\infty} w_m$, must satisfy the following condition

$$\lim_{m\to\infty} \left| \frac{w_{m+1}}{w_m} \right| < 1, \tag{39}$$

From (14), it can be seen that the CDF expression $F_{\tilde{\gamma}_j^{(r)}}(\cdot)$ consists of two infinite series and the CDF can be rewritten as

$$F_{\tilde{\gamma}_j^{(r)}}(x) = \underbrace{\frac{B_j K_1}{r\pi^2} \sum_{n=0}^{\infty} \frac{2^{P_1} K_2^{-\frac{1}{2}}}{n!} G_{1j} G_{1\,2}^{1\,1}\left(\frac{K_2 x^{\frac{2}{r}}}{\gamma_0^{\frac{2}{r}}} \middle| \begin{matrix} 1 \\ \frac{n+1}{2}, 0 \end{matrix} \right)}_{S_1} + 1 - \underbrace{\frac{B_j K_1}{2\pi^2} \sum_{n=0}^{\infty} \frac{2^{P_1} K_2^{-\frac{1}{2}}}{n!} G_{1j} \Gamma\left(\frac{n+1}{2}\right)}_{S_2}. \tag{40}$$

Further, the series coefficients $w_n^{(1)}$ and $w_n^{(2)}$ of the two individual series S_1 and S_2, respectively, are given by

$$w_n^{(1)} = \frac{2^{n+P_2}}{n!} G_{10\;3}^{1\;10}\left(\frac{2^8 K_2 \delta^2}{C_j} \middle| \begin{matrix} \mathcal{X}_{3j} \\ \left[\frac{n}{2}, \frac{-\rho_j}{2}, \frac{1-\alpha_{2j}}{2}\right] \end{matrix} \right) \times G_{1\,2}^{1\,1}\left(\frac{K_2 x^{\frac{2}{r}}}{\gamma_0^{\frac{2}{r}}} \middle| \begin{matrix} 1 \\ \frac{n+1}{2}, 0 \end{matrix} \right), \tag{41}$$

$$w_n^{(2)} = \frac{2^{n+P_2}}{n!} G_{10\;3}^{1\;10}\left(\frac{2^8 K_2 \delta^2}{C_j} \middle| \begin{matrix} \mathcal{X}_{3j} \\ \left[\frac{n}{2}, \frac{-\rho_j}{2}, \frac{1-\alpha_{2j}}{2}\right] \end{matrix} \right) \times \Gamma\left(\frac{n+1}{2}\right). \tag{42}$$

From (39), the ratios of the coefficients can be expressed as

$$\lim_{n\to\infty} \left| \frac{w_{n+1}^{(2)}}{w_n^{(2)}} \right| = \lim_{n\to\infty} \frac{\frac{2^{n+1+P_2}}{(n+1))!}}{\frac{2^{n+P_2}}{n!}} M_1 \times M_2 = \lim_{n\to\infty} \frac{2M_1 M_2}{n}, \tag{43}$$

$$\lim_{n\to\infty} \left| \frac{w_{n+1}^{(2)}}{w_n^{(2)}} \right| = \lim_{n\to\infty} \frac{\frac{2^{n+1+P_2}}{(n+1)!}\Gamma\left(\frac{n+2}{2}\right)}{\frac{2^{n+P_2}}{n!}\Gamma\left(\frac{n+1}{2}\right)} M_1 = \lim_{n\to\infty} \frac{2M_1 \Gamma\left(\frac{n+2}{2}\right)}{n\Gamma\left(\frac{n+1}{2}\right)}, \tag{44}$$

where $M_1 = \frac{G_{10\;3}^{1\;10}\left(\frac{2^8 K_2 \delta^2}{C_j} \middle| \begin{matrix} \mathcal{X}_{3j} \\ \left[\frac{n+1}{2}, \frac{-\rho_j}{2}, \frac{1-\alpha_{2j}}{2}\right] \end{matrix} \right)}{G_{10\;3}^{1\;10}\left(\frac{2^8 K_2 \delta^2}{C_j} \middle| \begin{matrix} \mathcal{X}_{3j} \\ \left[\frac{n}{2}, \frac{-\rho_j}{2}, \frac{1-\alpha_{2j}}{2}\right] \end{matrix} \right)}$ and $M_2 = \frac{G_{1\,2}^{1\,1}\left(\frac{K_2 x^{\frac{2}{r}}}{\gamma_0^{\frac{2}{r}}} \middle| \begin{matrix} 1 \\ \frac{n+2}{2}, 0 \end{matrix} \right)}{G_{1\,2}^{1\,1}\left(\frac{K_2 x^{\frac{2}{r}}}{\gamma_0^{\frac{2}{r}}} \middle| \begin{matrix} 1 \\ \frac{n+1}{2}, 0 \end{matrix} \right)}$ will always be the constants for all real values of n. Furthermore, it is evident that the exponents of the denominators in both (43) and (44) are greater than the exponents of the numerators. Thus, by taking the limit as $n \to \infty$, the coefficients of the series will tend to zero. Hence, it can be concluded that the final expressions of outage and ASER, which are derived from (14), are absolutely convergent.

This article has been accepted for publication in IEEE Internet of Things Journal. This is the author's version which has not been fully edited and
content may change prior to final publication. Citation information: DOI 10.1109/JIOT.2024.3455577

TABLE III: Simulation Parameters

Parameter	Value
Wavelength of the FSO signal, λ_F	1550 nm
Beam divergence angle, ϕ_{d_j}	2 mrad
Aperture radius, a_0	0.2 m
Correlation coefficient due to imperfect CSI, δ	0.9
Jitter standard deviation at the transmitter, σ_{θ_j}	0.0008
Jitter standard deviation at the ORS, σ_{φ_j}	0.0001
Modulation index, $\mathcal{M}$	2
Detection technique parameter, r	2
Link distances, $L_{1j} = L_{2j}$	150 m

TABLE IV: Truncation accuracy of the infinite sum given in (27) and (32)

γ_0	Final values of outage (27) for truncation limit n				Upper limit
	40	80	120	140	
20	0.113627	0.113599	0.113595	0.113595	$n=120$
30	0.045194	0.045180	0.045178	0.045178	$n=120$
40	0.032127	0.032116	0.032115	0.032114	$n=120$

γ_0	Final values of ASER (32) for truncation limit n				Upper limit
	40	80	120	140	
20	0.022437	0.022430	0.022429	0.022429	$n=120$
30	0.015875	0.015869	0.015868	0.015868	$n=120$
40	0.014275	0.014270	0.014269	0.014269	$n=120$

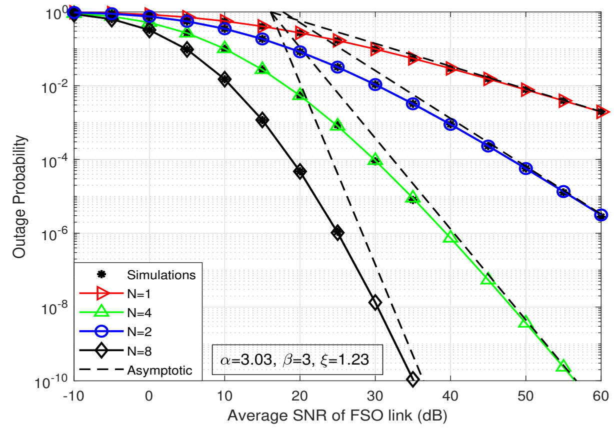

Fig. 2: Outage probability for different number of ORSs under perfect CSI

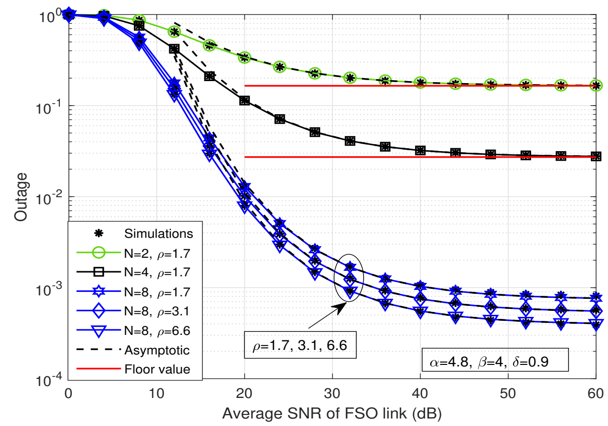

Fig. 3: Outage probability for various ORSs under imperfect CSI

V. Numerical and Simulation Results

The simulation and analytical results for ASER and outage probability are presented in this section. The values of the parameters assumed in the simulations are given in Table III. Further, the parameter values in Table III are consistently assumed for both the source to the j^{th} ORS and the j^{th} ORS to the destination links. This simplification, represented as $\rho_j = \rho$, $\alpha_{2j} = \alpha_{1j} = \alpha$, and $\beta_{2j} = \beta_{1j} = \beta$, is made without loss of generality. The simulations were conducted using MATLAB R2021b on a personal computer equipped with an Intel i7 processor running at 4.70 GHz and 32GB of RAM. This setup ensured that our simulations were performed efficiently, allowing for the accurate modeling of the system's performance under the specified conditions.

The truncation accuracy for infinite summations used in (27) and (32) are listed in Table IV. In addition, if the values greater than the upper limits are applied for truncating the infinite series, then it will not alter the fifth decimal figure of final outage and ASER values.

Fig. 2 and Fig. 3 show the outage performance for different number of ORSs under perfect and imperfect CSI, respectively. It is observed from the plots that increasing N considerably improves the outage of the system, since the outage performance directly depends on N as given by (28). Furthermore, in Fig. 2, the SNR gain obtained by varying N from $N = 1$ (single ORS-assisted FSO) to $N = 2$ is 18 dB for an outage probability of 10^{-2}. Similarly, when the number of ORSs is increased from $N = 2$ to $N = 4$, the SNR gain obtained is 12 dB and the SNR gain from $N = 4$ to $N = 8$ is 8 dB. Additionally, in Fig. 3, the outage performance is also shown for different pointing errors at $N = 8$ and it is observed that the performance of the system improves with increase in ρ. This is because, higher values of ρ represents lower severity of pointing errors, which results in better system performance.

In Fig. 4 and Fig. 5, the ASER performances are presented for different number of ORSs under perfect CSI and imperfect CSI, respectively. Similar to outage probability plots, it is evident that by increasing N, the ASER performance of the system also improves significantly for both the cases. Additionally, in Fig. 4, the performance of the proposed multiple ORSs-assisted system is compared with the multiple parallel relay-aided system assuming decode-and-forward (DF) protocol. It is inferred from the plots that the ASER performance of multiple ORS systems is better than that of multiple relay-aided systems when the average SNRs are below 14.5, 17, and 19 dB for $N = 1, 2,$ and 3 respectively, which are also the points of intersection. However, after the points of intersection, the relay-aided system outperforms the ORS-assisted system. This is because, the impact of decoding errors in the relay-aided system is more dominant below the points of intersection, and with increasing SNR, the decoding errors reduce significantly. Furthermore, as the value of N increases, the diversity and reliability of the ORS-assisted system improve.

This article has been accepted for publication in IEEE Internet of Things Journal. This is the author's version which has not been fully edited and
content may change prior to final publication. Citation information: DOI 10.1109/JIOT.2024.3455577

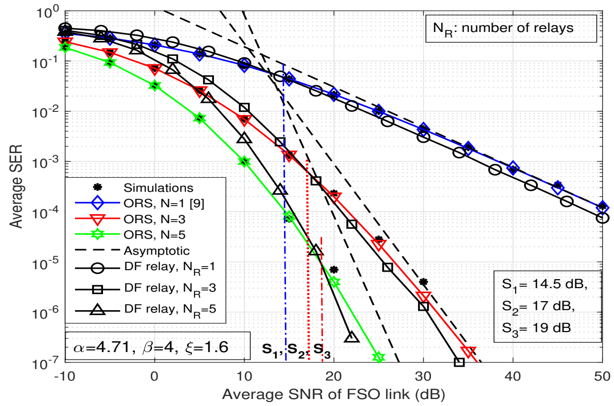

Fig. 4: Average SER performance for different number of ORSs under perfect CSI

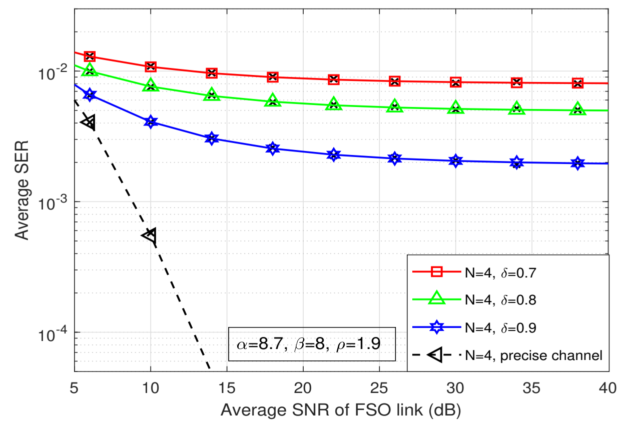

Fig. 6: ASER performance for various correlation coefficients

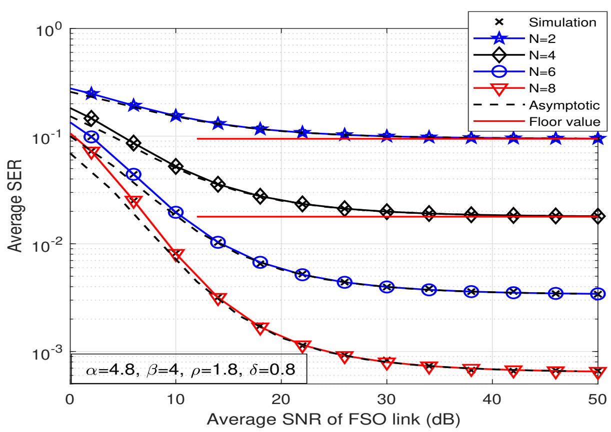

Fig. 5: ASER performance for different number of ORSs under imperfect CSI

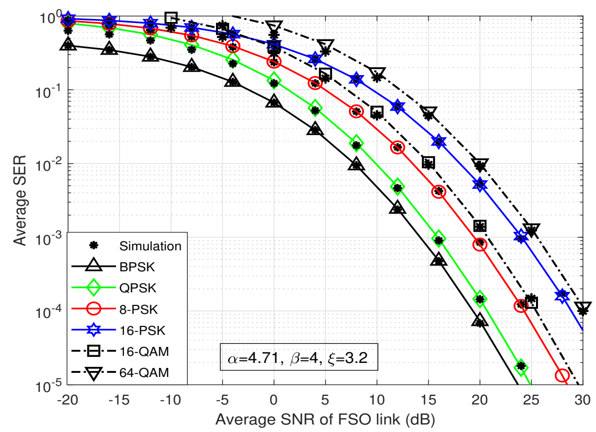

Fig. 7: Average SER performance for different modulation techniques under perfect CSI

This shifts the demarcation point to different SNR levels, indicating the SNR region where the relay-based system begins to outperform the ORS-assisted system. However, it deserves to be noted that ORSs are passive nodes that do not require a dedicated energy source for RF processing, decoding, and encoding, unlike relay nodes.

It is also noticed from the outage and ASER performances in Fig. 3 and 5 that the curves are saturated at high-SNR region and attain outage and ASER floor values equal to P_0^{fixed} and P_{ser}^{fixed} as mentioned in Section IV-A and IV-B. For example, at 56 dB SNR, the values of P_0^{fixed} inferred from Fig. 3 for $N = 2$ and 4 are 0.1671 and 0.0279, respectively, which are nearly equal to its values, 0.1649 and 0.0271, obtained from (30). Likewise, P_{ser}^{fixed} values observed from Fig. 5 for $N = 2$, 4 are 0.0952 and 0.0181 at 46 dB SNR. The values of P_{ser}^{fixed} calculated using (38) are 0.0944 and 0.0178, which are also almost equivalent to those obtained from Fig. 5. Furthermore, it is evident from Fig. 2, Fig. 3, Fig. 4, and Fig. 5 that the simulation results intently coincide with the analytical results, which approves our derived outage and ASER expressions. Additionally, the asymptotic results in Fig. 2, Fig. 3, Fig. 4, and Fig. 5 are intently concurring with the analytical results at the high-SNR region, which affirms the accuracy of the asymptotic analysis.

In Fig. 6, the ASER performance is shown for imperfect CSI with correlation coefficient $\delta = 0.7, 0.8, 0.9$ and perfect CSI case with $\delta = 1$. It is seen that the increasing values of correlation coefficient enhances the ASER performance. For example, at $\gamma_0 = 22$ dB, the ASER values for $\delta = 0.7, 0.8, 0.9$ are $8.6 \times 10^{-3}, 5.5 \times 10^{-3}$, and 2.3×10^{-3}, respectively. It is due to the fact that high value of δ implies less errors in channel estimation.

Fig. 7 illustrates the ASER for various modulation techniques, namely BPSK, QPSK, 8-PSK, 16-PSK, 16-QAM, and 64-QAM, assuming $N = 3$ and perfect CSI. The ASER plots clearly indicate that the performance deteriorates as the modulation order $\mathcal{M}$ increases. In order to attain an ASER of 10^{-3}, BPSK requires an average SNR of 14 dB. Likewise, QPSK, 8-PSK, 16-QAM, 16-PSK, and 64-QAM require the average SNR values of 16 dB, 20 dB, 21 dB, 24 dB, and 26 dB, respectively. Additionally, 16-QAM tends to outperform 16-PSK in terms of ASER under the same conditions. Further, the simulation results closely match the analytical results, confirming the accuracy of the derived ASER. It is to be noted that SER expression serves as a tight upper bound for M-QAM and MPSK. However, it is worth noting that this upper bound is tighter for MPSK compared to M-QAM.

In Fig. 8, the outage performance of the proposed ORSs-assisted FSO system is compared for different turbulence conditions under imperfect CSI. From the plots, it is seen that the outage probability increases under strong turbulence

This article has been accepted for publication in IEEE Internet of Things Journal. This is the author's version which has not been fully edited and
content may change prior to final publication. Citation information: DOI 10.1109/JIOT.2024.3455577

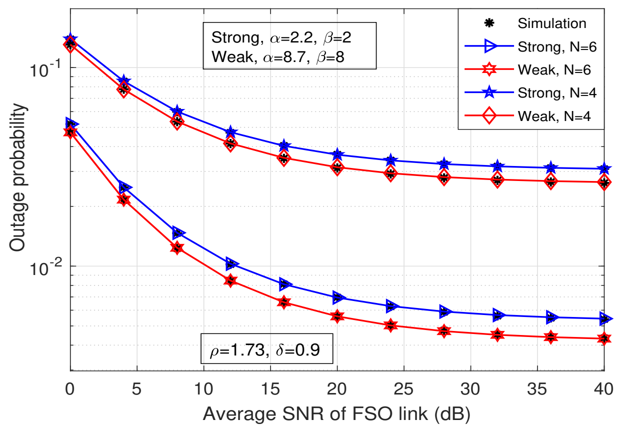

Fig. 8: Outage probability under different turbulence scenarios for imperfect CSI

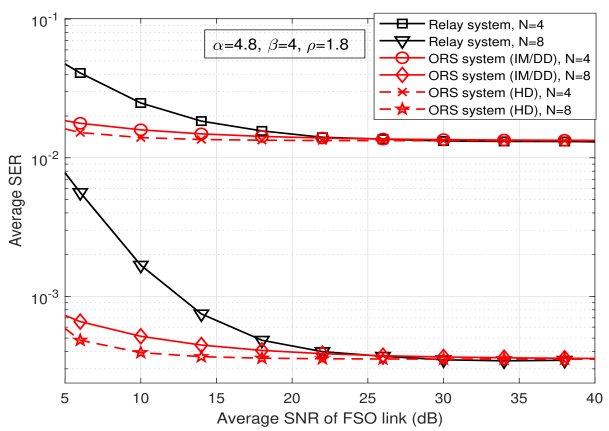

Fig. 9: ASER performance for different detection techniques under imperfect CSI

compared to weak turbulence, as expected. This is because, the random variations in the atmospheric channel are more evident in strong turbulence than in weak turbulence. Further, the performance of the proposed system improves under both strong and weak turbulence conditions with increasing number of ORSs, i.e., from $N = 4$ to $N = 6$. For instance, at 12 dB SNR, the outage probability values achieved under strong turbulence condition are 0.047 and 0.010 for $N = 4$ and $N = 6$, respectively. Similarly, for weak turbulence, the outage values obtained at 12 dB SNR are 0.041 and 0.008 for $N = 4$ and $N = 6$, respectively.

In Fig. 9, it is observed that the multiple ORSs-assisted FSO system performs better than the multiple parallel relay-aided FSO system, which utilizes DF relaying protocol with maximum instantaneous SNR-based relay selection technique, especially in the SNR region $\gamma_0 < 22$ dB. It is to be noted that similar trends have been observed in Fig. 4 with perfect CSI condition as well. Further, it can be seen from Fig. 9 that the relay-aided system achieves an ASER of 1.6×10^{-3} for $N = 8$ at $\gamma_0 = 10$ dB, whereas, for the same SNR, the ORS-assisted system attains very low ASER values of 5.1×10^{-4} and 3.9×10^{-4} under IM/DD and HD techniques, respectively This is because, the decoding errors effect in the DF relaying system dominate as compared to the cascaded channel effect in the ORS-assisted system, which in turn leads to degradation in the system performance of relay-based system. Further, due to coherent detection, the performance of the ORS system with HD technique is better than the IM/DD technique for both $N = 4$ and $N = 8$ cases.

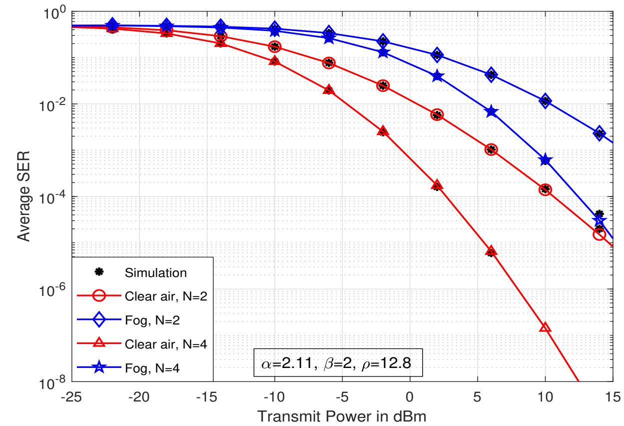

Fig. 10: Average SER for clear air and foggy conditions under perfect CSI

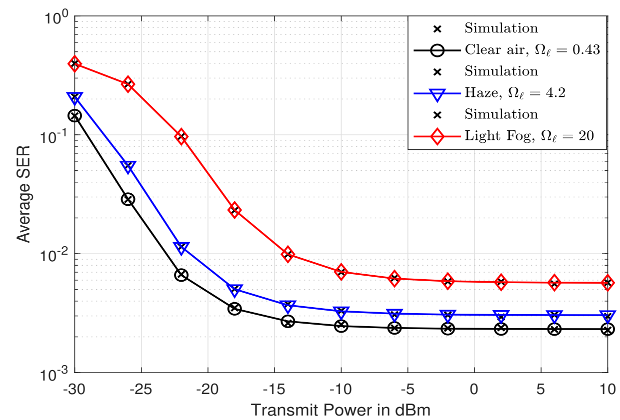

Fig. 11: Average SER for clear air and foggy conditions under imperfect CSI

In Fig. 10, the ASER is plotted against the transmit power under perfect CSI for clear air and light fog conditions. The values of the weather coefficient are assumed as $\Omega_\ell = 0.43$ and $\Omega_\ell = 20$ for clear air and light fog, respectively. It is clearly observed from the plots that the system performance degrades significantly from clear air to foggy conditions. This deterioration can be attributed to the susceptibility of FSO systems to foggy weather conditions. Moreover, significant improvement in the performance is obtained with transmit power gain of more than 5 dBm to attain the ASER of 10^{-2} under both clear air and foggy conditions as the number of ORSs increase from $N = 4$ to $N = 6$. Finally, in Fig. 11, the ASER is plotted against the transmit power for imperfect CSI case under different weather conditions, including clear air, haze, and fog. The ASER plots show a noticeable degradation in system performance as the weather conditions change from clear air to fog due to the same reason stated earlier.

VI. Conclusions and Future Works

In this paper, a multiple ORSs-aided FSO system was proposed to alleviate the LOS condition in the FSO link and and to improve performance in comparison to the existing single

ORS-based FSO system and FSO system without ORS. The proposed ORSs-aided FSO system was examined considering a selection scheme, which selects the best ORS for transmission. Further, the modeling of the FSO channel incorporates atmospheric turbulence, attenuation, pointing errors, and the presence of imperfect CSI conditions. The unified closed-form expressions for the PDF and CDF of instantaneous SNR of the overall channel were derived for both perfect and imperfect CSI conditions. Capitalizing on the PDF and CDF expressions, the outage probability and ASER performances were obtained using the derived statistical functions. In addition, an asymptotic analysis was conducted at high-SNR region to determine the diversity gain of the system and we also performed a convergence test on the obtained analytical expressions comprising the infinite series. Through asymptotic analysis, it can be inferred that the diversity gain of the multiple ORSs system depends on the number of ORSs and turbulence parameters. From the numerical results, it was observed that the performance of the proposed multiple ORSs-aided FSO system improves with the usage of more number of reflecting surfaces in both perfect and imperfect CSI cases. Furthermore, multiple ORSs-assisted FSO system outperformed multiple DF-relaying-aided FSO system, without necessitating extra signal processing and power requirements. Consequently, the ORS-aided FSO system shall be introduced as a promising alternative to the multi-DF-relaying-based FSO systems. Our study demonstrates that the turbulence, pointing errors, and imperfect CSI is crucial for analyzing the performance of the proposed ORS-assisted FSO system. Increasing the number of ORSs and improving the CSI accuracy significantly enhance the system performance and reliability, providing essential insights for future system designs.

In future work, we plan to enhance the proposed multiple ORSs-assisted FSO system by incorporating multiple reflecting elements in each ORS to further improve the SNR of the overall system. We will develop a comprehensive model that accounts for an arbitrary number of reflecting elements in ORSs. Additionally, we will analyze the system's performance by considering practical factors, such as atmospheric turbulence, pointing errors, and weather attenuation. Furthermore, we will explore the impact of hardware impairments, imperfect CSI, and imperfect phase compensation of ORS on the multiple ORSs-assisted FSO system, as these factors are critical in realistic scenarios.

Appendix A
Proof of Theorem 1

From (8), let us assume $\tilde{I}_j = D + E$ as the sum of two independent random variables, where $D = \delta I_j$ and $E = \sqrt{1-\delta^2}\epsilon$. Furthermore, the PDF of E is given by

$$f_E(y) = K_1 \exp\left(-K_2 y^2\right), \tag{45}$$

where $K_1 = \frac{1}{\sqrt{2\pi(1-\delta^2)\sigma_e^2}}$ and $K_2 = \frac{1}{2(1-\delta^2)\sigma_e^2}$. Using the convolution theorem, we can write the PDF of $\tilde{I}_j$ as

$$f_{\tilde{I}_j}(t) = \int_0^\infty f_D(x) f_E(t-x) dx, \tag{46}$$

where $f_D(x) = \frac{1}{\delta} f_{I_j}\left(\frac{x}{\delta}\right)$. By substituting (45) in (46) and after writing the exponential function in (45) in terms of Meijer G-function using [44, 07.34.03.0228.01], we get the following integral

$$f_{\tilde{I}_j}(t) = B_j K_1 \exp\left(-K_2 t^2\right) \sum_{n=0}^{\infty} \frac{(2K_2)^n}{n!} t^n \times \int_0^\infty x^{n-1} G_{1\,5}^{5\,0}\left(\frac{C_j}{\delta}x \middle| \begin{matrix}\rho_j+1 \\ \mathcal{X}_{2j}\end{matrix}\right) G_{0\,1}^{1\,0}\left(K_2 x^2 \middle| 0\right) dx \tag{47}$$

Finally, by utilizing [44, 07.34.21.0013.01], the above integral is evaluated as

$$f_{\tilde{I}_j}(t) = \frac{B_j K_1}{\pi^2} \exp\left(-K_2 t^2\right) \sum_{n=0}^{\infty} \frac{2^{P_1} K_2^{\frac{n}{2}}}{n!} G_{1j} t^n \tag{48}$$

It can be observed from (8) that $\epsilon \in \mathcal{R}$. However, in case of a practical channel, the channel gain values are positive. Therefore, by assuming the negative channel values as zero [40], the PDF of $f_{\tilde{I}_j}(t)$ can be rewritten as

$$f_{\tilde{I}_j}(t) = \begin{cases} \frac{B_j K_1}{\pi^2} \exp\left(-K_2 t^2\right) \sum\limits_{n=0}^{\infty} \frac{2^{P_1} K_2^{\frac{n}{2}}}{n!} G_{1j} t^n, & t > 0 \\ 1 - I_0^{(j)}, & t = 0. \end{cases} \tag{49}$$

where $I_0^{(j)}$ can be calculated as

$$I_0^{(j)} = \int_0^\infty f_{\tilde{I}_j}(t) dt \tag{50}$$

After substituting (48) in place of $f_{\tilde{I}_j}(t)$ in (50), we get

$$I_0^{(j)} = \frac{B_j K_1}{\pi^2} \sum_{n=0}^{\infty} \frac{2^{P_1} K_2^{\frac{n}{2}}}{n!} G_{1j} \int_0^\infty t^n \exp\left(-K_2 t^2\right) dt \tag{51}$$

By utilizing [43, eq. (3.381.4)], $I_0^{(j)}$ is obtained as

$$I_0^{(j)} = \frac{B_j K_1}{2\pi^2} \sum_{n=0}^{\infty} \frac{2^{P_1} K_2^{-\frac{1}{2}}}{n!} G_{1j} \Gamma\left(\frac{n+1}{2}\right) \tag{52}$$

Appendix B
Proof of Theorem 2

From (15), probability that the maximum instantaneous SNR $\gamma_{\max}$ is less than γ can be written as

$$\begin{aligned} \Pr(\gamma_{\max} < \gamma) &= \Pr(\max\{\gamma_1^{(r)}, \cdots, \gamma_N^{(r)}\} < \gamma) \\ &= \Pr(\gamma_1^{(r)} < \gamma, \cdots, \gamma_N^{(r)} < \gamma) \end{aligned} \tag{53}$$

Since we have assumed that each of the ORS-based FSO links are non-identical and independent of each other, the probability expression in (53) can be further simplified as

$$\Pr(\gamma_{\max} < \gamma) = \prod_{j=1}^{N} \Pr(\gamma_1^{(r)} < \gamma) \Pr(\gamma_2^{(r)} < \gamma) \cdots \Pr(\gamma_N^{(r)} < \gamma) \tag{54}$$

By replacing the $\Pr(\cdot)$ with the corresponding CDF expression $F_{\gamma_j^{(r)}}(\cdot)$, the CDF is written as

$$\Pr(\gamma_{\max} < \gamma) = F_{\gamma_{\max}}(\gamma) = \prod_{j=1}^{N} F_{\gamma_j^{(r)}}(\gamma) \tag{55}$$

Furthermore, by substituting the CDF expression in (55) with (12), the final expression for $F_{\gamma_{max}}(\gamma)$ can be written as

$$F_{\gamma_{max}}(\gamma) = \prod_{j=1}^{N} B_j G^{\,5\,1}_{\,2\,6} \left(C_j \left(\frac{\gamma}{\gamma_0} \right)^{\frac{1}{r}} \middle| \begin{matrix} 1, \rho_j + 1 \\ \mathcal{X}_{2j}, 0 \end{matrix} \right) \tag{56}$$

References

[1] E. Basar and I. Yildirim, "Reconfigurable intelligent surfaces for future wireless networks: A channel modeling perspective," *IEEE Wireless Commun.*, vol. 28, no. 3, pp. 108–114, 2021.

[2] E. Basar, M. D. Renzo, J. De Rosny, M. Debbah, M. Alouini, and R. Zhang, "Wireless communications through reconfigurable intelligent surfaces," *IEEE Access*, vol. 7, pp. 116 753–116 773, 2019.

[3] V. D. P. *et al*, "Performance of cooperative communication system with multiple reconfigurable intelligent surfaces over Nakagami-m fading channels," *IEEE Access*, vol. 10, pp. 9806–9816, 2022.

[4] M. Di Renzo, A. Zappone, M. Debbah, M.-S. Alouini, C. Yuen, J. de Rosny, and S. Tretyakov, "Smart radio environments empowered by reconfigurable intelligent surfaces: How it works, state of research, and the road ahead," *IEEE J. Sel. Areas Commun.*, vol. 38, no. 11, pp. 2450–2525, 2020.

[5] D. Tyrovolas, S. A. Tegos, E. C. Dimitriadou-Panidou, P. D. Diamantoulakis, C. K. Liaskos, and G. K. Karagiannidis, "Performance analysis of cascaded reconfigurable intelligent surface networks," *IEEE Wireless Commun. Lett.*, vol. 11, no. 9, pp. 1855–1859, 2022.

[6] N. P. Le and M.-S. Alouini, "Performance analysis of RIS-aided THz wireless systems over α-μ fading: An approximate closed-form approach," *IEEE Internet of Things Journal*, pp. 1–1, 2023.

[7] Q. Wu, S. Zhang, B. Zheng, C. You, and R. Zhang, "Intelligent reflecting surface-aided wireless communications: A tutorial," *IEEE Trans. Commun.*, vol. 69, no. 5, pp. 3313–3351, 2021.

[8] Z. Ghassemlooy, S. Arnon, M. Uysal, Z. Xu, and J. Cheng, "Emerging optical wireless communications-advances and challenges," *IEEE J. Sel. Areas Commun.*, vol. 33, no. 9, pp. 1738–1749, 2015.

[9] S. A. Al-Gailani, M. F. Mohd Salleh, A. A. Salem, R. Q. Shaddad, U. U. Sheikh, N. A. Algeelani, and T. A. Almohamad, "A survey of free space optics (FSO) communication systems, links, and networks," *IEEE Access*, vol. 9, pp. 7353–7373, 2021.

[10] M. Z. Chowdhury, M. K. Hasan, M. Shahjalal, M. T. Hossan, and Y. M. Jang, "Optical wireless hybrid networks: Trends, opportunities, challenges, and research directions," *IEEE Commun. Surveys Tuts.*, vol. 22, no. 2, pp. 930–966, 2020.

[11] A. S. Hamza, J. S. Deogun, and D. R. Alexander, "Classification framework for free space optical communication links and systems," *IEEE Commun. Surveys Tuts.*, vol. 21, no. 2, pp. 1346–1382, 2019.

[12] G. Yang, M.-A. Khalighi, Z. Ghassemlooy, and S. Bourennane, "Performance evaluation of receive-diversity free-space optical communications over correlated Gamma–Gamma fading channels," *Appl. Opt.*, vol. 52, no. 24, pp. 5903–5911, Aug 2013.

[13] M. Safari and M. Uysal, "Relay-assisted free-space optical communication," *IEEE Trans. Wireless Commun.*, vol. 7, no. 12, pp. 5441–5449, 2008.

[14] S. Malik and P. K. Sahu, "M-ary phase-shift keying-based single-input-multiple-output free space optical communication system with pointing errors over a Gamma–Gamma fading channel," *Appl. Opt.*, vol. 59, no. 1, pp. 59–67, Jan 2020.

[15] H. Kazemi and M. Uysal, "Performance analysis of MIMO free-space optical communication systems with selection combining," in *Proc. 21st Signal Processing and Communications Applications Conference (SIU)*, 2013, pp. 1–4.

[16] E. Zedini, H. Soury, and M.-S. Alouini, "Dual-hop FSO transmission systems over Gamma–Gamma turbulence with pointing errors," *IEEE Trans. Wireless Commun.*, vol. 16, no. 2, pp. 784–796, 2017.

[17] E. Zedini and M.-S. Alouini, "On the performance of multihop heterodyne FSO systems with pointing errors," *IEEE Photon. J.*, vol. 7, no. 2, pp. 1–10, 2015.

[18] S. Anees and M. R. Bhatnagar, "Performance evaluation of decode-and-forward dual-hop asymmetric radio frequency-free space optical communication system," *IET Optoelectron.*, vol. 9, no. 5, pp. 232–240, 2015.

[19] N. Vishwakarma and Swaminathan R., "Performance analysis of hybrid FSO/RF communication over generalized fading models," *Optics Commun.*, vol. 487, p. 126796, 2021.

[20] S. Sharma, A. S. Madhukumar, and Swaminathan R., "MIMO hybrid FSO/RF system over generalized fading channels," *IEEE Veh. Technol. Mag.*, vol. 70, no. 11, pp. 11 565–11 581, 2021.

[21] P. Bhardwaj, V. Bansal, N. Biyani, S. Shukla, and S. M. Zafaruddin, "Performance of integrated IoT network with hybrid mmWave/FSO/THz backhaul link," *IEEE Internet of Things Journal*, pp. 1–1, 2023.

[22] H. Wang, Z. Zhang, B. Zhu, J. Dang, L. Wu, L. Wang, K. Zhang, Y. Zhang, and G. Y. Li, "Performance analysis of multi-branch reconfigurable intelligent surfaces-assisted optical wireless communication system in environment with obstacles," *IEEE Veh. Technol. Mag.*, vol. 70, no. 10, pp. 9986–10 001, 2021.

[23] V. Jamali, H. Ajam, M. Najafi, B. Schmauss, R. Schober, and H. V. Poor, "Intelligent reflecting surface assisted free-space optical communications," *IEEE Commun. Mag.*, vol. 59, no. 10, pp. 57–63, 2021.

[24] M. Di Renzo, K. Ntontin, J. Song, F. H. Danufane, X. Qian, F. Lazarakis, J. De Rosny, D.-T. Phan-Huy, O. Simeone, R. Zhang, M. Debbah, G. Lerosey, M. Fink, S. Tretyakov, and S. Shamai, "Reconfigurable intelligent surfaces vs. relaying: Differences, similarities, and performance comparison," *IEEE Open Journal of the Communications Society*, vol. 1, pp. 798–807, 2020.

[25] Y. Elsawy, A. S. Alatawi, M. Abaza, A. Moawad, and E.-H. M. Aggoune, "Next-generation dual transceiver FSO communication system for high-speed trains in Neom smart city," *Photonics*, vol. 11, no. 5, 2024.

[26] P. Agheli, H. Beyranvand, and M. J. Emadi, "High-speed trains access connectivity through RIS-assisted fso communications," *J. Lightwave Technol.*, vol. 40, no. 21, pp. 7084–7094, Nov 2022.

[27] M. Najafi, B. Schmauss, and R. Schober, "Intelligent reflecting surfaces for free space optical communication systems," *IEEE Trans. Commun.*, vol. 69, no. 9, pp. 6134–6151, 2021.

[28] H. Ajam, M. Najafi, V. Jamali, B. Schmauss, and R. Schober, "Modeling and design of IRS-assisted multilink FSO systems," *IEEE Transactions on Communications*, vol. 70, no. 5, pp. 3333–3349, 2022.

[29] A. R. Ndjiongue, T. M. N. Ngatched, O. A. Dobre, A. G. Armada, and H. Haas, "Analysis of RIS-based terrestrial-FSO link over G-G turbulence with distance and jitter ratios," *J. Lightw. Technol.*, vol. 39, no. 21, pp. 6746–6758, 2021.

[30] R. P. Naik, P. Krishnan, and G. D. G. Simha, "Reconfigurable intelligent surface-assisted free-space optical communication system under the influence of signal blockage for smart-city applications," *Appl. Opt.*, vol. 61, no. 20, pp. 5957–5964, Jul 2022.

[31] V. K. Chapala and S. M. Zafaruddin, "Unified performance analysis of reconfigurable intelligent surface empowered free-space optical communications," *IEEE Trans. Commun.*, vol. 70, no. 4, pp. 2575–2592, 2022.

[32] H. D. Le, T. V. Nguyen, and A. T. Pham, "Aerial IRS-aided vertical backhaul FSO networks over Fisher-Snedecor $\mathcal{F}$ turbulence channels," in *Proc. IEEE Ninth International Conference on Communications and Electronics (ICCE)*, 2022, pp. 133–138.

[33] S. Uniyal, N. Vishwakarma, and R. Swaminathan, "Multihop IRS-assisted free space optics communication with DF relaying: a performance analysis," *Appl. Opt.*, vol. 62, no. 18, pp. 4716–4726, Jun 2023.

[34] N. Vishwakarma, R. Swaminathan, P. D. Diamantoulakis, and G. K. Karagiannidis, "Performance analysis of optical reflecting surface-assisted optical space shift keying-based MIMO-FSO system," *IEEE Transactions on Communications*, vol. 71, no. 8, pp. 4751–4763, 2023.

[35] A. M. Salhab and L. Yang, "Mixed RF/FSO relay networks: RIS-equipped RF source vs RIS-aided RF source," *IEEE Wireless Commun. Lett.*, vol. 10, no. 8, pp. 1712–1716, 2021.

[36] S. Sharma, N. Vishwakarma, and R. Swaminathan, "Performance analysis of IRS-assisted hybrid FSO/RF communication system," in *Proc. National Conference on Communications (NCC)*, 2022, pp. 268–273.

[37] H. Lei, H. Luo, K.-H. Park, Z. Ren, G. Pan, and M. Alouini, "Secrecy outage analysis of mixed RF-FSO systems with channel imperfection," *IEEE Photon. J.*, vol. 10, no. 3, pp. 1–13, 2018.

[38] A. A. Ibrahim, S. Özgür Ata, E. Erdoğan, and L. Durak-Ata, "Performance analysis of free space optical communication systems over imprecise Malaga fading channels," *Optics Commun.*, vol. 457, p. 124694, 2020.

[39] N. Mensi and D. B. Rawat, "Reconfigurable intelligent surface selection for wireless vehicular communications," *IEEE Wireless Commun. Lett.*, vol. 11, no. 8, pp. 1743–1747, 2022.

[40] L. Han, X. Liu, Y. Wang, and B. Li, "Joint impact of channel estimation errors and pointing errors on FSO communication systems over $\mathcal{F}$ turbulence channel," *J. Lightw. Technol.*, vol. 40, no. 14, pp. 4555–4561, 2022.

[41] L. Han, X. Liu, Y. Wang, and X. Hao, "Analysis of RIS-assisted FSO systems over $\mathcal{F}$ turbulence channel with pointing errors and imperfect

CSI," *IEEE Wireless Commun. Lett.*, vol. 11, no. 9, pp. 1940–1944, 2022.

[42] N. Vishwakarma and Swaminathan R., "Performance analysis of multiple optical reflecting surfaces assisted FSO communication," in *Proc. IEEE Wireless Communications and Networking Conference (WCNC)*, 2023, pp. 1–6.

[43] I. S. Gradshteyn and I. M. Ryzhik, *Table of Integrals, Series, and Products*. 7th ed.: Academic, 2007.

[44] Wolfram Research Inc., "Mathematica edition: Version 8," https://functions.wolfram.com/HypergeometricFunctions/MeijerG/, Champaign, IL, USA, 2010.

[45] A. Goldsmith, *Wireless communications*. Cambridge university press, 2005.

[46] A. M. Mathai, R. Saxena, and H. Haubold, *The H-Function Theory and Applications*. New York: Springer, 2010.

[47] R. J. Sasiela, *Electromagnetic Wave Propagation in Turbulence*. Springer Science & Business Media, 12 2012.

[48] P. Concus, D. Cassatt, G. Jaehnig, and E. Melby, "Tables for the evaluation of $\int_0^\infty x^\beta e^{-x} f(x) dx$ by Gauss-Laguerre quadrature," *Mathematics of Computation*, vol. 17, no. 83, pp. 245–256, 1963.